

## 9. POST-EOCENE RECORD OF EOLIAN DEPOSITION AT SITES 752, 754, AND 756, EASTERN INDIAN OCEAN<sup>1</sup>

Steven A. Hovan<sup>2</sup> and David K. Rea<sup>2</sup>

### ABSTRACT

The late Cenozoic history of eolian sedimentation in the eastern Indian Ocean was developed from samples recovered during drilling of Sites 752, 754, and 756. Temporal changes in the mass accumulation rate of eolian material reflect major climatic shifts in the southern African source region. A significant drop in dust mass flux values occurs near the end of the lower Oligocene. Younger sediments are characterized by a gradual reduction in dust accumulation rates until the middle Miocene after which values remain consistently low throughout the late Cenozoic, although a slight increase in eolian accumulation rate occurs near 2.5 Ma. This pattern of dust mass flux appears related to the supply of dust-sized particles in the source region and represents a shift in the climatic regime of southern Africa to increasingly more arid conditions throughout the late Cenozoic.

### INTRODUCTION

A major objective of Ocean Drilling Program (ODP) Leg 121 was to investigate spatial and temporal paleoclimatic changes using sediments recovered in the eastern Indian Ocean. Changes in the mass flux of eolian dust result from changes in the supply of dust-sized particles at the eolian source region and are related to the climatic character of the source region (Pye, 1989). Sediments recovered during Leg 121 (Fig. 1) provide an opportunity to study Cenozoic changes in continental climate conditions of the Southern Hemisphere and measure their response to major global events like the development of large ice sheets over Antarctica and the Arctic Ocean.

In the pelagic ocean, away from the influence of hemipelagic, turbidite, and ice-rafting depositional processes, the terrigenous component of sediments is predominantly eolian dust (Ferguson et al., 1970; Leinen and Heath, 1981; Leinen et al., 1986). Most of this material originates in semi-arid to arid regions of continents and is transported long distances in the middle to upper troposphere by zonal wind systems. Temporal changes in the mass flux of dust to the ocean are primarily controlled by the supply of material in the source region. For shorter time scales on the order of years up to perhaps 500 k.y., arid to humid changes in the source region climate are responsible for variations in the mass flux of dust (Prospero et al., 1981; Rea et al., 1985; Prospero and Nees, 1986; Hovan et al., 1989). On longer time scales, the flux of eolian dust is related not only to regional climatic conditions (Fig. 2) but also to the overall supply of deflatable dust material on the continent (Pye, 1989). That is, both climatic shifts from humid to arid and from hyperarid to arid result in increased dust fluxes from the source region because each create conditions that form more fine-grained sedimentary particles available for transport. Sustained arid climatic conditions allow depletion of the supply of dust-sized particles in the source region. Thus, arid regions like southern Africa and Australia, although climatically conducive to being a major source of eolian transported material, actually produce very low fluxes of continental dust since the supply of dust-sized particles from those regions has been de-

pleted for millions of years (Lancaster, 1984; Prospero, 1985). As significant changes in the supply of dust particles occur in the source region during major shifts in climatic conditions, eolian sediments from the eastern Indian Ocean should provide a general paleoclimatic history of the Australian or African source regions, recording both the timing of major climatic changes and the temporal stability of climate regimes.

### METHODS

The eolian component was isolated using a series of chemical extractions as detailed by Rea and Janecek (1981). Carbonates were removed by treating each sample with a weak acetic acid solution. A buffered sodium citrate and sodium hydrosulfide solution was used to remove oxides, hydroxides, and zeolites, and warm sodium carbonate baths were used to dissolve biogenic silica. The resulting precision of this method determined from duplicate analyses is approximately  $\pm 5\%$ . Since this procedure does not remove volcanogenic material, smear slides were made for each of the extracted samples to provide semiquantitative, visual estimates of the amount of volcanic material present. Extracted samples containing a large proportion of volcanic material are noted in the text; the quantity of the total extracted sample less volcanogenic material is taken to be the terrigenous eolian material.

The mass accumulation rate (MAR) of eolian material to the seafloor can be determined by multiplying the weight percentage of eolian material by the linear sedimentation rate (LSR) and dry-bulk density (DBD) for each sample:

$$\text{Eolian MAR [mg (cm}^2 \text{ k.y.)}^{-1}] = \% \text{ extracted} \cdot \text{LSR (cm k.y.}^{-1}) \cdot \text{DBD [g (cm}^3 \text{)}^{-1}] \cdot 1000$$

Linear sedimentation rates were determined using Leg 121 nannofossil zonations (Peirce, Weissel, et al., 1989) and geochronology of Berggren et al. (1985). The dry-bulk density of each sample was calculated from porosity values measured from the bulk sediment water content.

### RESULTS

During drilling on Broken Ridge at Sites 752 and 754 (Fig. 1), we recovered sediments consisting of foraminifer or foraminifer-bearing nannofossil ooze deposited from the late Eocene through the Pleistocene. A disconformity at about 30 Ma separates an

<sup>1</sup> Weissel, J., Peirce, J., Taylor, E., Alt, J., et al., 1991. *Proc. ODP, Sci. Results, 121*; College Station, TX (Ocean Drilling Program).

<sup>2</sup> Department of Geological Sciences, The University of Michigan, Ann Arbor, MI 48109-1063, U.S.A.

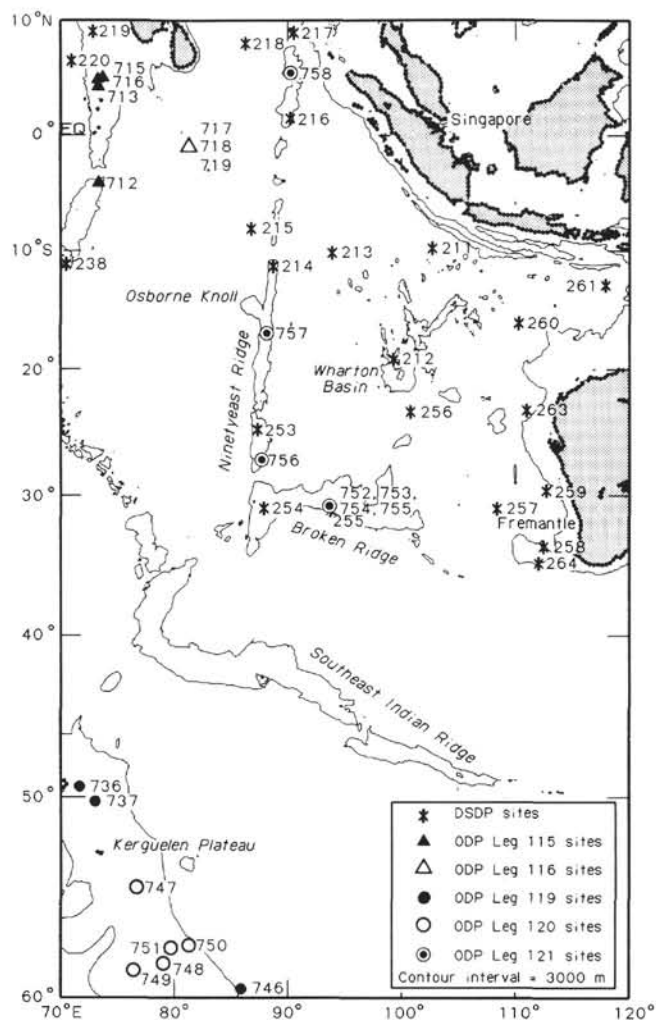


Figure 1. Index map of the eastern Indian Ocean showing the location of Leg 121 drill sites, as well as other ODP/DSDP drill sites in the eastern Indian Ocean.

apparently complete Neogene section from upper Eocene pelagic ooze (Peirce, Weissel, et al., 1989). Sediments recovered from Site 756 on Ninetyeast Ridge (Fig. 1) range in age from early Oligocene to Pleistocene and are dominantly nannofossil ooze with foraminifer contents varying between 5% and 20% (Peirce, Weissel, et al., 1989). Linear sedimentation rates at all three sites were generally low throughout the cored intervals varying between 1.1 cm/k.y. and 0.2 cm/k.y., with the lowest values occurring during the late Oligocene and Miocene (Tables 1, 2, and 3).

Extracted material percentages never exceed 10% by weight of the total sediment (Figs. 3 and 4; Tables 1, 2, and 3). Since the extracted fraction contains a combination of both continental dust and volcanogenic material, smear slides were made for each extracted sample to identify which samples contained a significant volcanic component. Large spikes of increased abundance of extracted material occur near the end of the early Miocene and are related to input of volcanic material. The remaining samples contain no appreciable volcanogenic contamination. In general, sediments from the Oligocene and lower Miocene sections contain the greatest percentage of dust. Abundances gradually declined throughout this period until the middle Miocene, and dust concentrations and fluxes remained consistently low for the rest of the Cenozoic (Figs. 3 and 4). Sediments from Sites 752 and 754

show a two-fold increase in eolian percentages at about 2.5 Ma coincident with an upper Pliocene  $\delta^{18}\text{O}$  enrichment (Fig. 3). The mass accumulation rate of extracted material ranges between about 0.1 and 35  $\text{mg}(\text{cm}^2 \text{k.y.})^{-1}$  and exhibits the same general features observed in the percentage data. The eolian flux record from Site 754, however, displays an additional increase from about 50 to 60 mbsf which is not present in the percentage data but occurs in conjunction with higher LSR values for that interval.

### IMPLICATIONS OF THE EOLIAN RECORD

The most striking characteristic of the eolian flux pattern in sediments of Sites 752, 754, and 756 is the extremely low rate of accumulation throughout most of the late Cenozoic. These low rates appear to characterize the Southern Hemisphere; similarly low dust fluxes were observed in Deep Sea Drilling Project (DSDP) Legs 91 and 92 sediments from the southeast Pacific Ocean (Schramm and Leinen, 1987; Bloomstine and Rea, 1986). Eolian sediments from the North Pacific, however, accumulate at rates 1 or 2 orders of magnitude greater than their Southern Hemisphere counterparts (Rea and Janecek, 1982; Rea et al., 1990) reflecting the overall decreased availability of fine sedimentary particles in Southern Hemisphere source regions. Temporal changes in the supply of dust-sized particles in the source region are the primary control over the late Cenozoic pattern of dust accumulation in the pelagic ocean. Paleoposition reconstructions show crust at Site 756 originated during the late Eocene near 50°S and slowly drifted northward to its present latitude near 27°S (Peirce, Weissel, et al., 1989). Sites 752 and 754 similarly drifted northward to their present positions near 31°S during this interval. Provided past zonal wind circulation patterns were similar to the present, most of the dust deposited at these sites would have been transported from the vast desert regions of southern Africa by westerly upper tropospheric winds (Oort, 1983). Thus, accumulated eolian material at these sites most likely provides a distal record of the supply of fine-grained sedimentary particles from southern Africa.

The Oligocene record of eolian accumulation is characterized by a marked drop in dust flux at the end of the early Oligocene (Fig. 4). Although this change occurs near an age boundary, the decrease in eolian percentages during this interval suggests that it is not simply an artifact of our age model (Fig. 4; Table 3). Thus, an important change must have occurred in the source region of eolian dust at the beginning of the late Oligocene which severely reduced the amount of fine sedimentary particles available for eolian transport. Pye (1989) suggests that a reduction in dust flux will occur if regional climatic conditions shift from either semi-arid to more humid or from arid to more arid (Fig. 2). Studies involving the sediments and landforms of southern African desert regions suggest arid to semi-arid conditions have prevailed throughout much of the past 20 Ma and possibly much longer (Lancaster, 1981). Thus, the reduction in dust flux values at the end of the lower Oligocene appears to represent a sustained shift to more arid climatic conditions in the southern Africa eolian source region.

After the major flux decrease at the end of the early Oligocene, dust accumulation rates continued to decline gradually during the late Oligocene and early Miocene (Figs. 3 and 4) until the middle Miocene when eolian accumulation rates dropped to extremely low values generally less than 1.5  $\text{mg}(\text{cm}^2 \text{k.y.})^{-1}$  and remained consistently low until the present. The eolian record at Site 754 shows a period of higher accumulation rates during the middle Miocene. Since the eolian percentage data from Site 754 correlate well with the eolian percentage records from Sites 752 and 756 and show no increase at this time (Figs. 3 and 4), this portion of the eolian accumulation record probably reflects differences in the calculated linear sedimentation rates and may not represent a

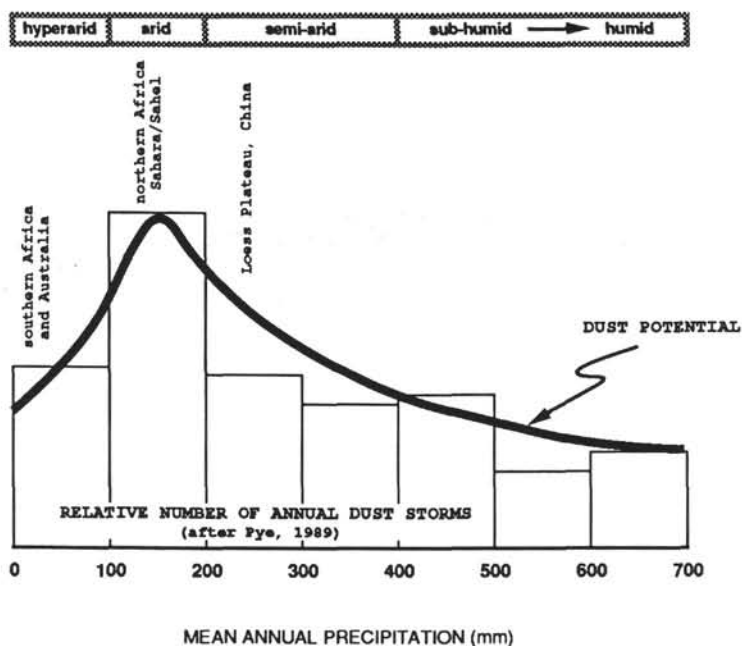


Figure 2. Schematic diagram representing the relationship between dust production and climate in the source region.

true increase in the input of eolian material to Site 754. Thus, the middle Miocene reduction in dust accumulation coincides with a large increase in  $\delta^{18}\text{O}$  associated with ice volume growth on Antarctica (Figs. 3 and 4) and apparently marks a further shift to greater aridity in southern African climate (Fig. 2). Extremely low dust accumulation rates since the middle Miocene imply that the eolian source region has remained under stable hyperarid conditions, essentially "blown dry" of dust particles, throughout much of the entire late Cenozoic. Eolian accumulation rates increase slightly near 2.5 Ma reflecting a greater supply of dust particles in southern Africa as would occur during a shift to relatively less arid regional climate conditions. Lancaster (1981, 1984) identified a Quaternary increase in annual rainfall throughout the Kalahari region of southern Africa based on extensive dune systems which have become fixed by savanna vegetation. These climatic changes occur coincident with late Pliocene continental ice growth reflected in the  $\delta^{18}\text{O}$  record (Fig. 3).

The major spikes in extracted percentage and flux values for the middle Miocene (Figs. 3 and 4) are associated with input of volcanogenic material and reported for these sediments (Peirce, Weissel, et al., 1989). X-ray diffraction analysis of samples from Site 756 (Sample 121-756B-6H-5, 30–35 cm) showed them to be composed mainly of two types of volcanic material, smectitic clays, and calcic plagioclase grains (Fig. 5). The size of the plagioclase grains ranges from 10  $\mu\text{m}$  to 175  $\mu\text{m}$ . A large abundance of grains this size cannot be explained by normal atmospheric transport processes and may reflect a local source or nearby erosional reworking of previously deposited basaltic-volcanogenic material.

### CONCLUSIONS

Isolation and analysis of eolian material in sediments from Sites 752, 754, and 756 provide a distal record of paleoclimatic variation in the southern Africa eolian source region. Temporal variations in the mass flux of dust suggest that climatic conditions in southern Africa shifted to more arid conditions near the beginning of the late Oligocene. Regional climates experienced a further shift to hyperaridity during the middle Miocene. Such

conditions appear to have prevailed for much of the late Cenozoic except for a slight decrease in aridity near 2.5 Ma.

### ACKNOWLEDGMENTS

We thank Tom Janecek and Eric Barron for reviews of this manuscript. Janice Pappas was responsible for eolian extractions from the Broken Ridge samples. This work was supported by funds from JOI-USSAC and from the National Science Foundation via grant no. OCE-8811299.

### REFERENCES

- Berggren, W. A., Kent, D. V., Flynn, J. J., and Van Couvering, J. A., 1985. Cenozoic geochronology. *Geol. Soc. Am. Bull.*, 96:1407–1418.
- Bloomstine, M. K., and Rea, D. K., 1986. Post-middle Oligocene eolian deposition from the trade winds of the southeast Pacific. In Leinen, M., Rea, D. K., et al., *Init. Repts. DSDP*, 92: Washington (U.S. Govt. Printing Office), 331–340.
- Ferguson, W. S., Griffin, J. J., and Goldberg, E. D., 1970. Atmospheric dusts from the North Pacific: a short note on long range eolian transport. *J. Geophys. Res.*, 75:1137–1139.
- Hovan, S. A., Rea, D. K., Pisias, N. G., and Shackleton, N. J., 1989. A direct link between the China loess and marine  $\delta^{18}\text{O}$  records: aeolian flux to the North Pacific. *Nature*, 340:296–298.
- Lancaster, N., 1981. Palaeoenvironmental implications of fixed dune systems in southern Africa. *Palaeogeogr., Palaeoclimatol., Palaeoecol.*, 33:327–346.
- \_\_\_\_\_, 1984. Aridity in southern Africa: age, origins and expression in landforms and sediments. In Vogel, J. C. (Ed.), *Late Cainozoic Palaeoclimates of the Southern Hemisphere*, Rotterdam (A. A. Balkema Publishers), 433–444.
- Leinen, M., Cwienk, D., Heath, G. R., Biscaye, P. E., Kolla, V., Thiede, J., and Dauphin, J. P., 1986. Distribution of biogenic silica and quartz in recent deep-sea sediments. *Geology*, 14:199–203.
- Leinen, M., and Heath, G. R., 1981. Sedimentary indicators of atmospheric circulation in the Northern Hemisphere during the Cenozoic. *Palaeogeogr., Palaeoclimatol., Palaeoecol.*, 36:1–21.
- Oort, A. H., 1983. Global atmospheric circulation statistics, 1958–1973. *NOAA Prof. Pap.*, 14:115–173.
- Peirce, J., Weissel, J., et al., 1989. *Proc. ODP, Init. Repts.*, 121: College Station, TX (Ocean Drilling Program).

- Prospero, J. M., 1985. Records of past continental climates in deep-sea sediments. *Nature*, 315:279–280.
- Prospero, J. M., Glaccum, R. A., and Nees, R. T., 1981. Atmospheric transport of soil dust from Africa to South America. *Nature*, 289:570–572.
- Prospero, J. M., and Nees, R. T., 1986. Impact of the North African drought and El Niño on mineral dust in the Barbados trade winds. *Nature*, 320:735–738.
- Pye, K., 1989. Processes of fine particle formation, dust source regions, and climatic changes. In Leinen, M., and Sarnthein, M. (Eds.), *Paleoclimatology and Paleometeorology: Modern and Past Patterns of Global Atmospheric Transport*: Boston (Kluwer Acad. Publ.), 3–30.
- Rea, D. K., Hovan, S. A., and Janecek, T. R., in press. Late Quaternary flux of eolian dust to the pelagic ocean. In Hay, W. W. (Ed.), *Geomaterial Fluxes, Glacial to Recent*. National Research Council, Washington (Nat. Acad. Sci. Press).
- Rea, D. K., and Janecek, T. R., 1981. Mass accumulation rates of the non-authigenic, inorganic, crystalline (eolian) component of deep-sea sediments from the western mid-Pacific Mountains, DSDP Site 463. In Theide, J., Vallier, T. L., et al. *Init. Repts. DSDP, 62*: Washington (U.S. Govt. Printing Office), 653–659.
- \_\_\_\_\_, 1982. Late Cenozoic changes in atmospheric circulation deduced from North Pacific eolian sediments. *Mar. Geol.*, 49:149–167.
- Rea, D. K., and Leinen, M., 1988. Asian aridity and the zonal westerlies: late Pleistocene and Holocene record of eolian deposition in the Northwest Pacific Ocean. *Palaeogeogr., Palaeoclimatol., Palaeoecol.*, 66:1–8.
- Rea, D. K., Leinen, M., and Janecek, T. R., 1985. Geologic approach to the long-term history of atmospheric circulation. *Science*, 227:721–725.
- Schramm, C. T., and Leinen, M., 1987. Eolian transport to Hole 595A from the Late Cretaceous through the Cenozoic. In Menard, H. W., Natland, J. H., Jordan, T. H., Orcutt, J. A., et al., *Init. Repts. DSDP, 91*: Washington (U.S. Govt. Printing Office), 469–473.

**Date of initial receipt: 7 March 1990**

**Date of acceptance: 3 October 1990**

**Ms 121B-125**

**Table 1. Data for calculating the mass accumulation rates of the extracted component in samples from Hole 752A.**

Core, section, interval (cm)	Depth (mbsf)	Linear sedimentation rate (cm/k.y.)	Dry-bulk density (g/cm <sup>3</sup> )	Extracted (%)	Extracted flux mg/(cm <sup>2</sup> k.y.)
121-752A-					
1H-1, 30-35	0.30	0.23	1.10	0.34	0.9
1H-2, 30-35	1.80	0.23	1.04	0.36	0.9
1H-3, 30-35	3.30	0.23	1.09	0.32	0.8
1H-4, 30-35	4.80	0.40	1.17	0.32	1.5
1H-5, 30-35	6.30	0.40	1.19	0.32	1.5
1H-6, 30-35	7.80	0.40	1.12	0.51	2.3
2H-1, 30-35	8.60	0.40	1.14	0.38	1.7
2H-2, 25-30	10.05	0.40	1.16	0.27	1.2
2H-3, 27-32	11.57	0.55	1.13	0.14	0.9
2H-4, 25-30	13.04	0.55	1.12	0.16	1.0
2H-5, 25-30	14.55	0.55	1.14	0.13	0.8
2H-6, 25-30	16.05	0.55	1.16	0.15	0.9
3H-1, 25-30	18.05	0.55	1.13	0.15	1.0
3H-2, 25-30	19.55	0.43	1.10	0.17	0.8
3H-3, 25-30	21.05	0.43	1.12	0.12	0.6
3H-5, 25-30	24.05	0.43	1.11	0.14	0.7
3H-6, 25-30	25.55	0.42	1.12	0.20	1.0
4H-1, 25-30	27.55	0.42	1.00	0.21	0.9
4H-2, 25-30	29.05	0.42	1.03	0.24	1.0
4H-4, 25-30	32.05	0.42	1.07	0.27	1.2
4H-5, 25-30	33.55	0.42	1.06	0.31	1.4
4H-6, 25-30	35.05	0.42	1.17	0.27	1.3
5H-1, 25-30	37.05	0.42	1.07	0.28	1.2
5H-2, 25-30	38.55	0.42	1.18	0.11	0.5
5H-3, 25-30	40.05	0.42	1.11	0.18	0.8
5H-4, 25-30	41.55	0.42	1.10	0.17	0.8
5H-5, 30-35	43.10	0.42	1.18	0.20	1.0
5H-6, 25-30	44.55	0.42	1.14	0.24	1.2
6H-1, 25-30	46.65	0.42	1.27	0.27	1.4
6H-2, 25-30	48.15	0.42	1.19	0.27	1.4
6H-3, 25-30	49.65	0.42	1.24	0.21	1.1
6H-4, 25-30	51.15	0.42	1.22	0.22	1.1
6H-5, 25-30	52.65	0.42	1.19	0.35	1.8
7H-1, 25-30	56.35	0.42	1.18	0.37	1.8
7H-2, 25-30	57.82	0.42	1.19	0.38	1.9
7H-3, 25-30	59.35	0.54	1.13	0.46	2.8
7H-4, 25-30	60.85	0.54	1.13	0.58	3.6
7H-5, 25-30	62.35	0.54	0.95	0.96	4.9
7H-6, 25-30	63.85	0.54	0.94	0.51	2.6
8H-1, 25-30	66.05	0.54	1.08	0.91	5.3
8H-2, 25-30	67.55	0.54	1.09	0.83	4.8
8H-3, 25-30	69.05	0.54	0.98	0.59	3.1
8H-4, 25-30	70.55	0.54	0.95	0.42	2.2
8H-5, 25-30	72.05	0.54	1.10	0.49	2.9
8H-6, 25-30	73.55	0.28	1.08	0.75	2.3
9H-1, 25-30	75.65	0.28	1.32	0.45	1.7
9H-2, 25-30	77.15	0.28	1.59	0.60	2.7
9H-3, 25-30	78.65	0.28	1.14	0.58	1.8
9H-4, 25-30	80.15	0.28	1.24	0.75	2.6
9H-5, 25-30	81.65	0.28	1.21	0.71	2.4
9H-6, 25-30	83.15	0.28	1.27	0.89	3.2
10H-1, 25-30	85.25	0.28	1.11	1.08	3.4
10H-2, 25-30	86.75	0.28	1.06	0.59	1.7
10H-3, 25-30	88.25	0.28	1.09	0.48	1.5
10H-4, 25-30	89.75	0.28	1.00	0.54	1.5
10H-5, 25-30	91.25	0.28	1.09	0.65	2.0
10H-6, 25-30	92.75	0.04	1.08	0.92	0.4

**Table 2. Data for calculating the mass accumulation rates of the extracted component in samples from Hole 754A.**

Core, section, interval (cm)	Depth (mbsf)	Linear sedimentation rate (cm/k.y.)	Dry-bulk density (g/cm <sup>3</sup> )	Extracted (%)	Extracted flux mg/(cm <sup>2</sup> k.y.)
121-754A-					
1H-1, 30-35	0.30	0.3	0.92	0.19	0.6
1H-2, 30-35	1.80	0.3	1.05	0.21	0.7
1H-3, 30-35	3.30	0.3	1.09	0.16	0.6
1H-4, 30-35	4.80	0.3	1.05	0.18	0.6
2H-1, 30-35	6.40	0.3	1.14	0.14	0.5
2H-2, 30-35	7.90	0.8	1.06	0.21	1.7
2H-3, 30-35	9.40	0.8	1.21	0.21	2.0
2H-4, 30-35	10.90	0.6	1.27	0.23	1.8
2H-5, 30-35	12.40	0.6	1.10	0.15	1.0
2H-6, 30-35	13.90	0.6	1.10	0.11	0.7
3H-1, 30-35	16.00	0.6	1.06	0.12	0.8
3H-2, 30-35	17.50	0.8	1.02	0.10	0.8
3H-3, 30-35	19.00	0.5	1.17	0.12	0.6
3H-4, 30-35	20.50	0.5	1.05	0.10	0.5
3H-5, 30-35	22.00	0.5	1.07	0.10	0.5
3H-6, 30-35	23.50	0.5	1.09	0.15	0.8
4H-1, 30-35	25.60	0.6	1.04	0.15	1.0
4H-2, 30-35	27.10	0.6	1.07	0.11	0.7
4H-3, 30-35	28.60	0.6	1.05	0.10	0.7
4H-4, 30-35	30.10	0.6	1.14	0.09	0.6
4H-5, 30-35	31.60	0.6	1.10	0.09	0.7
4H-6, 30-35	33.10	0.6	1.08	0.11	0.7
5H-1, 30-35	35.20	0.3	1.00	0.15	0.4
5H-2, 30-35	36.70	0.3	1.06	0.12	0.3
5H-3, 30-35	38.20	0.3	1.11	0.17	0.5
5H-4, 30-35	39.70	0.3	1.04	0.12	0.3
5H-5, 30-35	41.20	0.3	1.07	0.15	0.4
5H-6, 30-35	42.70	0.3	0.98	0.12	0.3
5H-7, 30-35	44.20	0.3	1.09	0.18	0.5
6H-1, 30-35	44.80	0.3	1.12	0.18	0.5
6H-2, 30-35	46.30	0.3	1.10	0.21	0.6
6H-3, 30-35	47.80	1.2	1.01	0.13	1.5
6H-4, 30-35	49.30	1.2	1.16	0.25	3.3
6H-5, 30-35	50.80	1.2	1.11	0.20	2.6
6H-6, 30-35	52.30	1.2	1.11	0.15	2.0
7H-1, 30-35	54.40	1.2	1.18	0.30	4.1
7H-2, 30-35	55.90	1.2	1.14	0.29	3.9
7H-3, 30-35	57.40	1.2	1.19	0.46	6.3
7H-4, 30-35	58.90	1.2	1.22	0.23	3.3
7H-5, 30-35	60.40	1.2	1.17	0.26	3.5
7H-6, 30-35	61.90	1.2	1.20	0.31	4.3
8H-1, 30-35	64.29	1.2	1.20	0.18	2.5
8H-2, 30-35	65.60	1.2	1.13	0.21	2.8
8H-3, 30-35	67.10	1.2	1.16	0.28	3.7
8H-4, 30-35	68.60	1.2	1.15	0.25	3.3
8H-5, 30-35	70.10	1.2	1.16	0.27	3.6
8H-6, 30-35	71.60	1.2	1.17	0.22	3.0
8H-7, 30-35	73.10	1.2	1.19	0.24	3.2
9H-2, 30-35	75.30	0.6	1.15	0.52	3.5
9H-3, 30-35	76.80	0.6	1.11	0.68	4.4
9H-4, 30-35	78.30	0.6	1.02	1.00	5.9
9H-5, 30-35	79.80	0.6	1.10	0.68	4.3
9H-6, 30-35	81.30	0.6	1.09	0.41	2.6
10H-2, 30-35	85.00	0.4	1.14	0.41	1.8
10H-3, 30-35	86.50	0.4	1.19	0.62	2.9
10H-5, 30-35	89.50	0.6	1.22	0.39	2.7
10H-6, 30-35	91.00	0.6	1.26	0.25	1.8
11H-1, 30-35	93.20	0.8	1.07	0.23	1.9
11H-2, 30-35	94.70	0.8	1.24	0.36	3.4
11H-3, 30-35	96.20	0.8	1.23	0.30	2.7
11H-4, 30-35	97.70	0.8	1.26	0.30	2.8
11H-6, 30-35	100.70	0.8	1.12	0.48	4.0
12H-1, 30-35	102.90	0.8	1.08	0.16	1.3
12H-2, 30-35	104.40	0.8	1.08	0.19	1.5
12H-3, 30-35	105.90	0.8	1.04	0.25	1.9
12H-4, 30-35	107.40	0.8	1.12	0.32	2.7
12H-5, 30-35	108.90	0.2	1.14	0.37	0.7
12H-6, 30-35	110.40	0.2	1.17	0.31	0.6
12H-7, 30-35	111.90	0.2	1.23	0.37	0.8
13X-1, 30-35	112.60	0.2	1.07	0.36	0.7
13X-2, 30-35	114.10	0.2	1.15	0.61	1.2
13X-3, 30-35	115.60	0.3	1.15	0.88	3.5

**Table 3. Data for calculating the mass accumulation rates of the extracted component in samples from Hole 756B.**

Core, section, interval (cm)	Depth (mbsf)	Linear sedimentation rate (cm/k.y.)	Dry-bulk density (g/cm <sup>3</sup> )	Extracted (%)	Extracted flux mg/(cm <sup>2</sup> k.y.)
121-756B-					
1H-1, 30-35	0.30	0.0	1.06	0.41	0.1
1H-2, 30-35	1.80	0.3	1.13	0.27	0.9
1H-3, 30-35	3.30	0.3	1.17	0.30	1.1
1H-4, 30-35	4.80	0.3	1.12	0.32	1.1
1H-5, 30-35	6.30	0.3	1.19	0.26	0.9
1H-6, 30-35	7.80	0.3	1.19	0.26	0.9
2H-1, 35-40	8.85	0.3	1.19	0.20	0.7
2H-2, 30-35	10.30	0.3	1.20	0.24	0.9
2H-3, 30-35	11.80	0.3	1.22	0.26	1.0
2H-4, 30-35	13.30	0.6	1.18	0.32	2.4
2H-5, 30-35	14.80	0.6	1.23	0.34	2.7
2H-6, 30-35	16.30	0.6	1.16	0.26	1.9
3H-1, 30-35	18.40	0.6	1.22	0.34	2.7
3H-2, 30-35	19.90	0.6	1.22	0.28	2.2
3H-3, 30-35	21.40	0.6	1.21	0.24	1.8
3H-4, 30-35	22.90	0.4	1.21	0.22	1.1
3H-5, 30-35	24.40	0.4	1.22	0.14	0.7
3H-6, 30-35	25.90	0.4	1.22	0.18	0.9
4H-1, 30-35	28.00	0.4	1.11	0.15	0.7
4H-2, 30-35	29.50	0.4	1.13	0.19	0.9
4H-3, 30-35	31.00	0.4	1.12	0.22	1.0
4H-4, 30-35	32.50	0.4	1.14	0.33	1.6
4H-5, 30-35	34.00	0.2	1.12	0.30	0.7
4H-6, 30-35	35.50	0.2	1.09	0.29	0.6
4H-7, 30-35	37.00	0.2	1.14	0.30	0.7
5H-1, 30-35	37.60	0.2	1.10	0.27	0.6
5H-2, 30-35	39.10	0.2	1.12	0.27	0.6
5H-3, 30-35	40.60	0.2	1.16	0.30	0.7
5H-4, 30-35	42.10	0.2	1.16	0.21	0.5
5H-5, 30-35	43.60	0.2	1.20	0.44	1.0
5H-6, 30-35	45.10	0.2	1.16	0.47	1.1
5H-7, 30-35	46.60	0.2	1.18	0.28	0.7
6H-1, 30-35	47.20	0.2	1.14	0.53	1.2
6H-2, 30-35	48.70	0.3	1.14	0.53	1.9
6H-3, 30-35	50.20	0.3	1.07	1.56	5.4
6H-4, 30-35	51.70	0.3	1.10	2.90	10.3
6H-5, 30-35	53.20	0.3	1.02	9.54	31.4
6H-6, 30-35	54.70	0.3	1.05	1.64	5.5
6H-7, 30-35	56.20	0.3	1.08	0.95	3.3
7H-1, 30-35	56.50	0.3	1.00	0.98	3.1
7H-2, 30-35	58.00	0.3	1.13	1.63	5.9
7H-3, 30-35	59.50	0.3	1.09	4.65	16.4
7H-4, 30-35	61.00	0.3	1.15	2.68	9.9
7H-5, 30-35	62.50	0.3	1.09	3.39	11.9
7H-6, 30-35	64.00	0.3	1.13	1.30	4.7
7H-7, 30-35	65.50	0.3	1.18	1.28	4.9
8H-1, 30-35	65.90	0.3	1.15	1.67	6.2
8H-2, 30-35	67.40	0.3	1.16	1.54	5.7
8H-3, 30-35	68.90	0.3	1.19	1.54	5.9
8H-4, 30-35	70.40	0.3	1.25	1.30	5.2
8H-5, 30-35	71.90	0.3	1.23	1.39	5.5
8H-6, 30-35	73.40	0.3	1.24	1.45	5.8
8H-7, 30-35	74.90	0.3	1.32	1.52	5.8
9H-1, 30-35	75.50	0.3	1.14	1.52	5.0
9H-2, 30-35	77.00	0.3	1.26	1.66	6.1
9H-3, 30-35	78.50	0.3	1.31	1.60	6.1
9H-4, 30-35	80.00	0.3	1.27	1.61	5.9
9H-5, 30-35	81.50	0.3	1.28	1.59	5.9
9H-6, 30-35	83.00	0.3	1.27	2.05	7.5
9H-7, 30-35	84.50	0.3	1.34	1.95	7.5
10H-1, 30-35	85.20	0.3	1.34	1.63	6.3
10H-2, 30-35	86.70	0.3	1.28	2.10	7.8
10H-3, 30-35	88.20	0.3	1.26	2.16	7.9
10H-4, 30-35	89.70	0.3	1.31	2.00	7.6
10H-5, 30-35	91.20	0.3	1.30	2.36	8.9
10H-6, 30-35	92.70	0.3	1.32	1.87	7.1
10H-7, 30-35	94.20	0.3	1.30	2.61	9.9
11H-1, 30-35	94.90	0.5	1.24	2.68	16.8
11H-2, 30-35	96.40	0.5	1.22	2.47	15.3
11H-3, 30-35	97.90	0.5	1.17	3.82	22.8
11H-4, 30-35	99.40	0.5	1.17	3.91	23.3
11H-5, 30-35	100.90	0.5	1.26	2.73	17.5
11H-6, 30-35	102.40	0.5	1.20	3.58	21.8
11H-7, 30-35	103.90	0.5	1.31	1.85	12.3

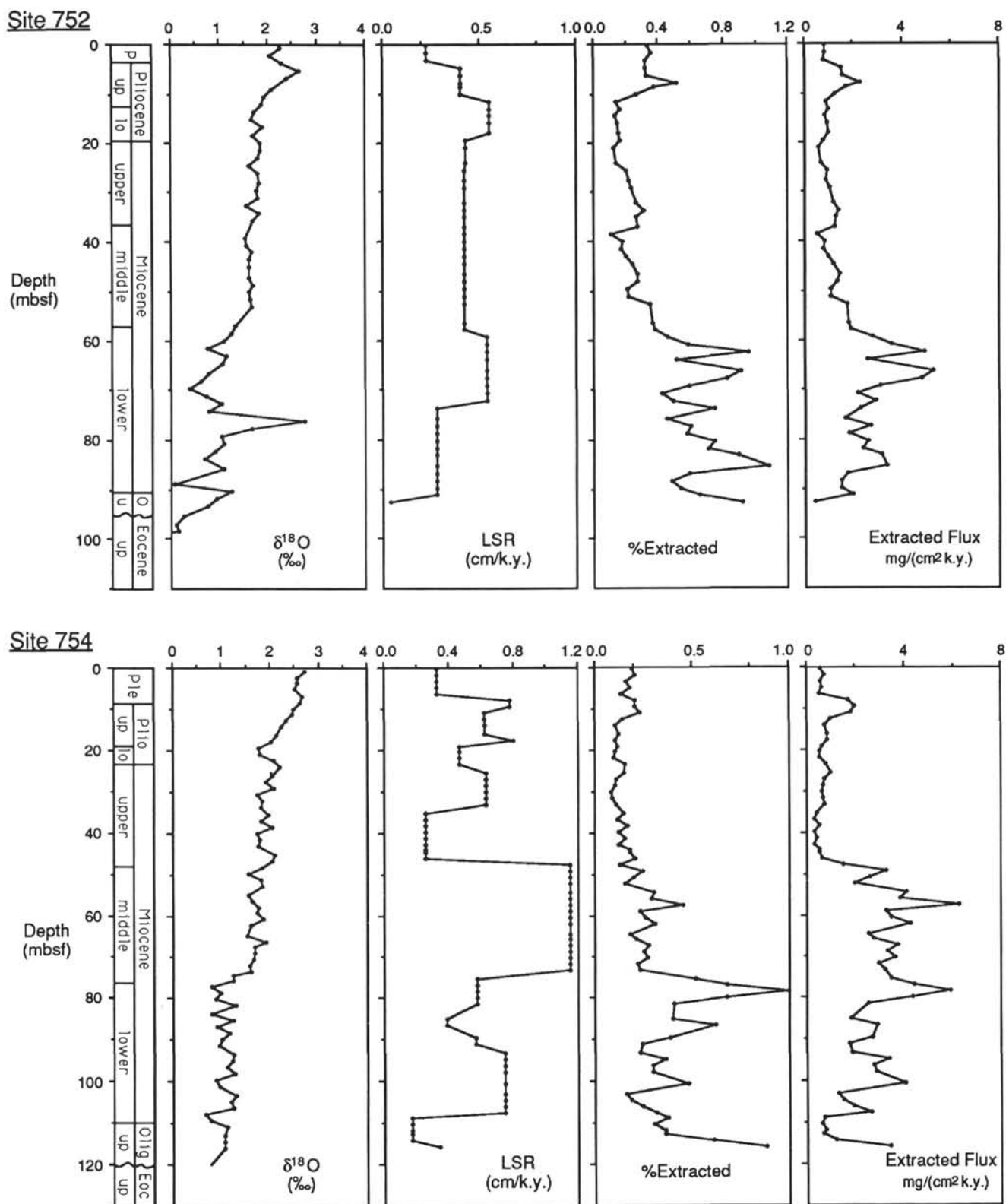


Figure 3. Variations in  $\delta^{18}\text{O}$ , linear sedimentation rate (LSR), and extracted sediment accumulation rates in samples from Sites 752 and 754.

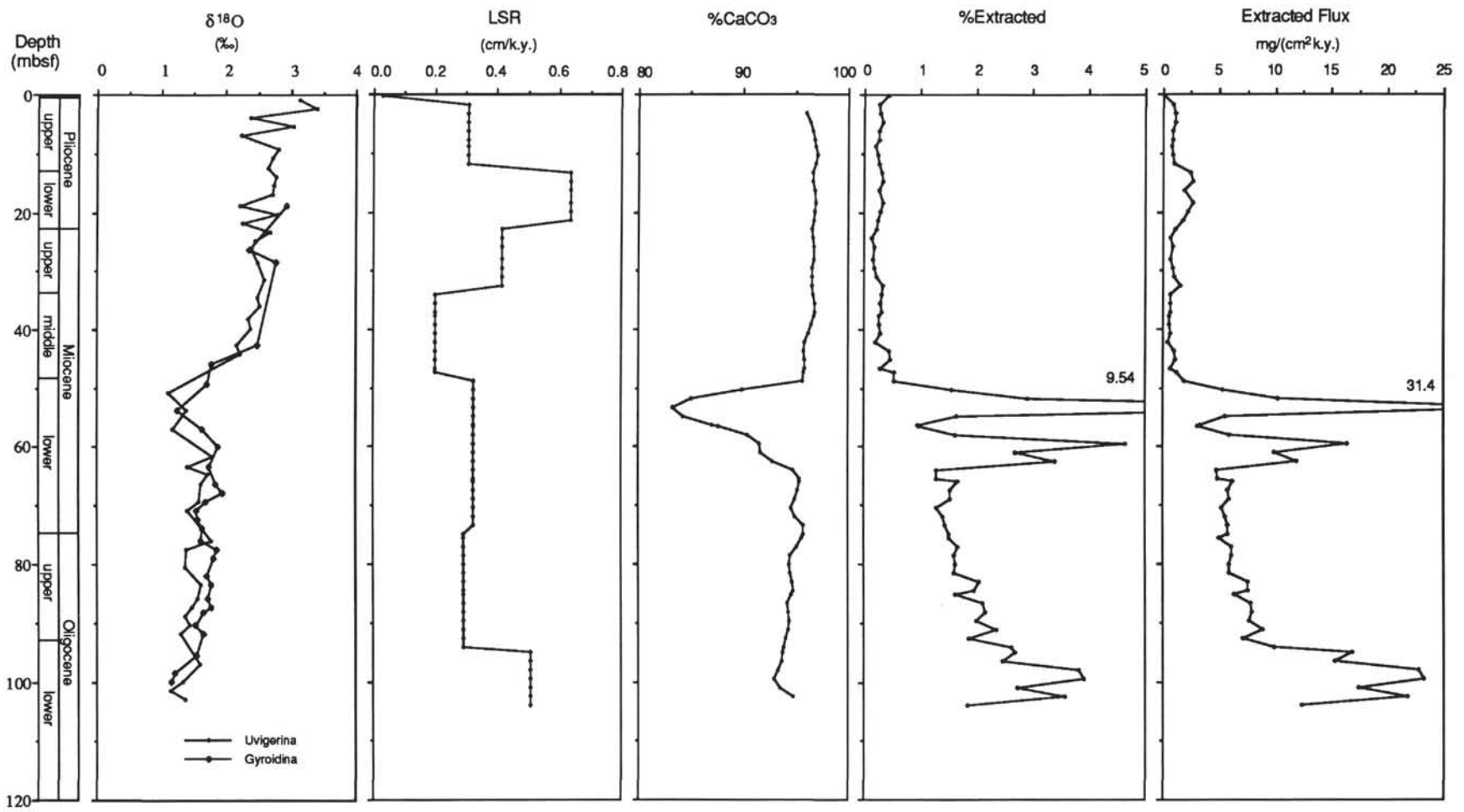
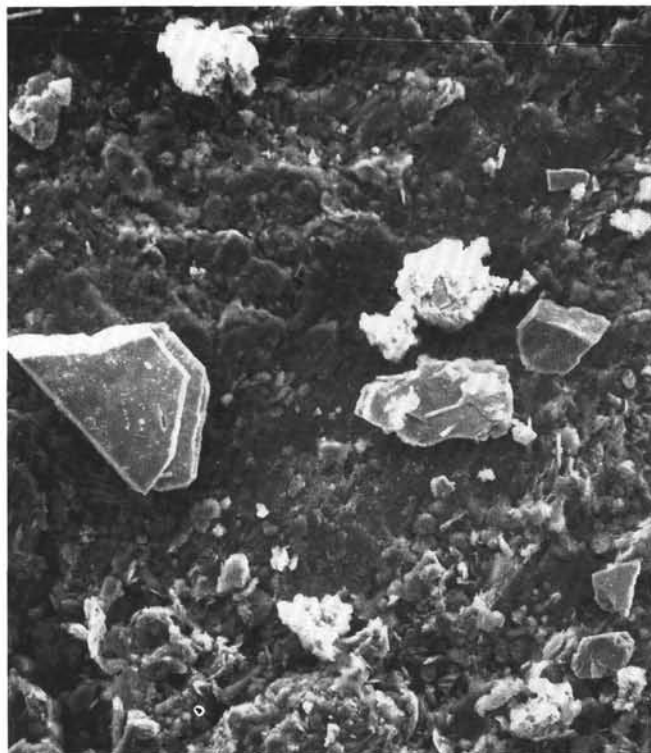


Figure 4. Variations in  $\delta^{18}\text{O}$ , LSR, CaCO<sub>3</sub> and extracted sediments in samples from Site 756. Oxygen isotope data from Rea et al. (this volume).



75  $\mu\text{m}$

Figure 5. Scanning electron microscopy (SEM) photograph of extracted material from Sample 121-756B-6H-5, 30-35 cm, 53.20 mbsf. The fine-grained component is dominated by smectitic clay particles. Larger, angular fragments are calcic plagioclase grains.